Preparation of Si quantum dots by phase transition with controlled annealing

IOP Publishing Journal Title
Journal **XX** (XXXX) XXXXXX https://doi.org/XXXX/XXXX

Preparation of Si quantum dots by phase transition with controlled annealing

Liyuan Fang,[1,3] Libin Tang, [2,3] *, Kar Seng Teng[4] *, Jinzhong Xiang[1,3]*

[1] School of Physical and Astronomy, Yunnan University, Kunming 650091, People's Republic of China
[2] Kunming Institute of Physics, Kunming 650223, People's Republic of China
[3] Yunnan Key Laboratory of Advanced Photoelectric Materials & Devices, No.31 East Jiaochang Road, 650223, Kunming, People's Republic of China
[4] College of Engineering, Swansea University, Bay Campus, Fabian Way, Swansea SA1 8EN, United Kingdom

E-mail: sscitang@163.com (L. B. Tang), k.s.teng@swansea.ac.uk (K. S. Teng), jzhxiang@ynu.edu.cn (J. Z. Xiang)

Received xxxxxx
Accepted for publication xxxxxx
Published xxxxxx

Abstract

Silicon quantum dots (Si-QDs) are excellent luminescent material due to its unique optoelectronic properties and have huge application potential in the field of photodetection. Recently, there has been much research interests in developing low-cost, facile and environmentally friendly methods to prepare the nanomaterials in addition to yielding excellent performances. In this article, we developed a novel preparation method of producing Si-QDs film based on carbon-silicon composite. The film was synthesized by co-sputtering using magnetron sputtering technique and studied at different annealing temperatures. Upon annealing, the film was transformed from an amorphous state to a crystalline state leading to Si-QDs precipitation, which can be observed at a low temperature of 600 °C. A Si-QDs thin film/n-Si photodetector was then prepared and characterized. The device exhibited a high specific detection rate (D^*) of 1.246×10^{12} cmHz$^{1/2}$W^{-1} under 940 nm (1.1 mWcm^{-2}) infrared radiation at 5 V bias. It also demonstrated good responsiveness and stability.

Keywords: Si-QDs, photodetector

1. Introduction

Nanomaterials have attracted much research interests and activities due to its quantum size effect[1], surface effect[2], small size effect[3] and macroscopic quantum tunneling effect[4] etc., which have demonstrated many applications in different scientific fields. Quantum dots (QDs) are one of the popular low-dimensional materials that have been researched extensively for applications in photovoltaics, biomedicine, and catalysis etc. Methods used to prepare these QDs include chemical precipitation[5], microemulsion[6], solvent-thermal[7], electrochemical etching[8], ion implantation[9], sputtering deposition[10] and so on.

Silicon is an environmentally friendly and low-cost narrow band gap semiconductor material. Interestingly, silicon quantum dots (Si-QDs) exhibit high luminous efficiency[11]. Furthermore, Si-QDs film demonstrates better uniformity and adhesion than solution and colloidal Si-QDs, therefore the Si-QDs film is considered as an excellent luminescent material that has led to application in photodetection[12]. At present, magnetron sputtering[10] and plasma-enhanced chemical vapor deposition (PECVD) [13]

techniques are two widely used methods to produce Si-QDs film. Magnetron sputtering is a simple physical deposition method that allows film formation at relatively low cost[14-16]. For example, Seifarth et al.[17] performed RF magnetron sputtering on Si single crystal to deposit SiO_x films at different substrate temperatures in Ar/O_2 environment, and then annealed the films at 1000 °C under N_2 environment, which resulted in the precipitation of QDs at the surface of the film after high temperature annealing for one hour. However, the high annealing temperature presents a great challenge in the preparation of Si-QDs films. These Si-QDs in the films are usually embedded in three commonly used substrates, such as SiO_2, SiN, and SiC, and different substrates would give rise to different optoelectronic properties of the Si-QDs films[18].

In this paper, a novel method of preparing Si-QDs films at low temperature is reported. The formation of QDs on quartz substrate at an annealing temperature of 600 °C was observed. The change mechanism of the film from amorphous state to precipitated QDs as the annealing temperature changes was systematically studied. A prototype photodetector based on the Si-QDs film was prepared and characterized. The film exhibited exceptional photoelectric properties that are suitable for high performance photodetection.

2. Experimental

Quartz substrate was first cleaned for film deposition by immersing it in a mixed solution of hydrogen peroxide, ammonia water and deionized water (1:1:3) at 80 °C for 30 mins, and then rinsed with deionized water and dried. Subsequently, a thin film was deposited onto the substrate at room temperature by co-sputtering C and n-Si targets using the magnetron sputtering technique. C as the barrier layer is beneficial to the preparation of Si-QDs. The RF and DC magnetron sputtering power for C and n-Si targets were 120 and 60 W, respectively. Film deposition was performed at a sputtering pressure of 0.68 Pa and argon gas flow of 50 sccm for 20 mins. The atomic concentration of C is listed as 37.7%, and the atomic concentration of Si is 52.6% (see Supplementary Figure S1).

3. Results and discussion

Crystal structure of the synthesized Si-QDs film is illustrated in Fig. (1)a. The deposited carbon-silicon composite film was annealed in a furnace at a pressure of 1.8 Pa at 600 °C for 1h. Upon annealing, the film changed from amorphous to crystalline and precipitated a large number of Si-QDs as well as a small number of structures consisting of crystalline Si and β-SiC (see Supplementary Figure S2), and the ratio of Si-QDs to β-SiC is approximately 6:1 (see Supplementary Figure S3). Si atom forms a covalent bond with its four adjacent atoms, which represent a diamond structure. β-SiC has a zinc blende structure, where one C and

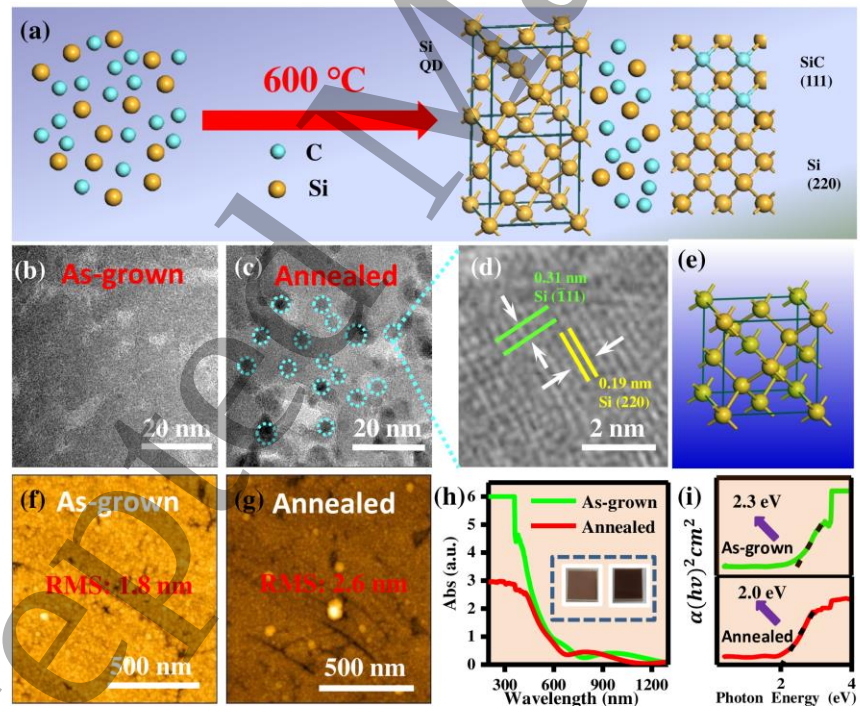

Figure 1. (a) Schematic diagram on crystal structure of the synthesized Si-QDs film. (b) and (c) TEM images of as-grown and annealed films, respectively. (d) HRTEM image showing lattice fringes from the selected area of (c). (e) Schematic diagram on crystal structure of Si-QDs. (f) and (g) AFM images of the Si-QDs film before and after annealing, respectively. (h) UV-Vis absorption spectra of the as-grown and annealed film. (Inset: optical images of as-grown (left) and annealed (right) films) (i) Optical band gap of the as-grown (top) and annealed (bottom) films.

four Si form a regular tetrahedral structure. The effect of annealing on the crystallinity of the film was studied by transmission electron microscope (TEM). Fig. 1(b) and 1(c) show high-resolution TEM (HRTEM) images of as-grown and annealed films, respectively. The as-grown film prepared by magnetron sputtering exhibited amorphous characteristics, while the annealed film revealed a large number of QDs having a grain size between 5 and 7 nm. The annealing temperature has a great effect on the formation of Si-QDs (see Supplementary Figure S4). Fig. 1(d) shows the lattice fringes of a quantum dot from the selected area of Fig. 1(c). The spacing of the lattice fringes were 0.19 and 0.31 nm, which correspond to the (220) and ($\bar{1}$11) crystal plane of Si, respectively, the result is consistent with the previous work reported in the literature[19]. Schematic diagram on the crystal structure of Si-QDs is depicted in Fig. 1(e). Fig. 1(f) and 1(g) are AFM images of the film before and after annealing, respectively. The surface of as-grown film has a relatively uniform root-mean-square (RMS) roughness of 1.8 nm. After annealing, the film experienced phase separation with nanocrystalline growth that resulted in an increased RMS roughness of 2.6 nm. UV-Vis absorption spectra of the film before and after annealing are shown in Fig. 1(h). The spectra showed absorption between visible light and infrared band. After annealing, the adsorption peak experienced red shift. Moreover, a significant reduction in the absorption peak at the visible light band was observed. The optical band gap (E_g) of the film can be calculated using the following formula:

$$\alpha(h\nu)=A(h\nu-E_g)^{1/2} \quad (1)$$

where α is molar absorption coefficient, h is Planck constant, v is frequency of incident photon, and A is a constant. As shown in Fig. 1(i), the optical band gaps of the as-grown and annealed films were calculated to be 2.3 eV and 2.0 eV, respectively, which suggests narrowing of the band gap due to the formation of Si-QDs after annealing of the film.

Fig. 2(a) and 2(e) show the AFM images of step edge between the deposited film and substrate before and after annealing with thickness of the film measured as 121 and 134 nm, respectively. The deposition rate of C and Si for the prepared film was approximately 6 nm per minute. X-ray photoelectron spectroscopy (XPS) was used to study the elemental composition and the effect of annealing on the carbon-silicon composite films. Fig. 2(b)-(d) and 2(f)-(h) show the XPS spectra of full scan, C 1s and Si 2p core level peaks before and after annealing, respectively. Comparing the full scan spectra in Fig. 2(b) and 2(f) show an increase in the Si 2p peak and a decrease in the C 1s peak after annealing. Most of the oxygen element was originated from the quartz substrate, however the sputtered film might also experience some degree of oxidation. The C 1s core level peak was deconvoluted into three Gaussian peaks situated at 282.4, 284.1 and 286.2 eV, which can be attributed to C-Si, C-C and C-O bonds, respectively[20]. The peak at 282.4 eV can be associated with the formation of SiC. The three deconvoluted Gaussian peaks of Si 2p at 98.88, 100.14 and102.31 eV can be attributed to Si-Si, C-Si and Si-O bonds, respectively[21]. The peak at 100.14 eV can be associated to

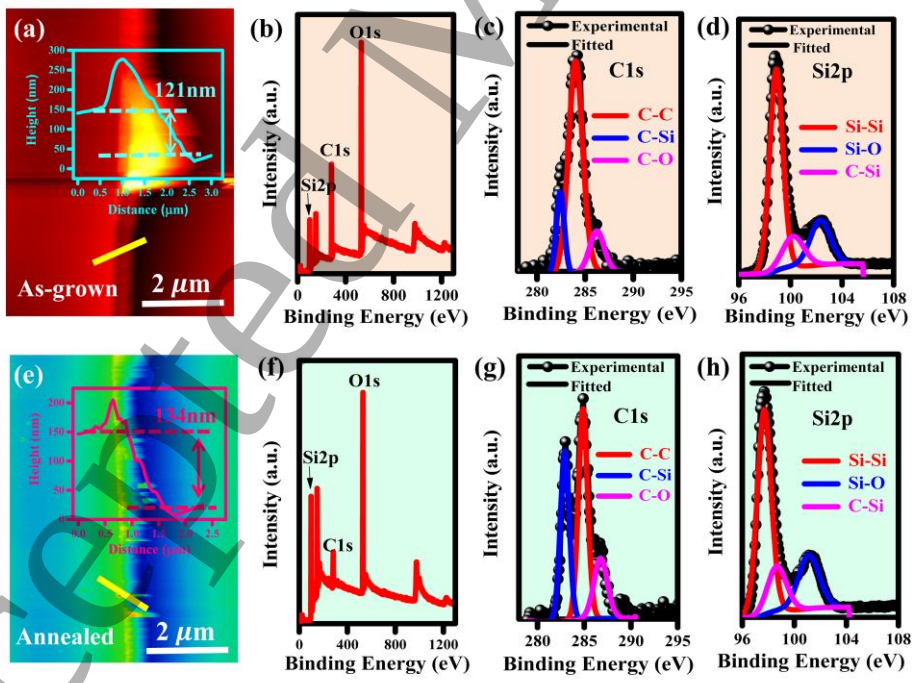

Figure 2. (a) and (e) AFM images on step edge between the deposited film and substrate of as-grown and annealed films, respectively. (b)-(d) XPS spectra showing full scan, C 1s and Si 2p core level peaks of as-grown film, respectively. (f)-(h) XPS spectra showing full scan, C 1s and Si 2p core level peaks of annealed film, respectively.

SiC formation, which is consistent with the deconvoluted peak in C 1s. After the sputtering of the film, under annealing Si atoms combine with each other to form Si crystal nuclei, then growing and forming of Si-QDs. The effect of increasing the annealing temperature to 900 °C on the precipitation of Si-QDs was investigated. HRTEM image oflin 900 °C (Supplementary Figure S4). Higher annealing temperature can cause Si atoms to react with C atoms and residual oxygen in the furnace, hence inhibiting the formation of Si-QDs, since $\triangle G_{\alpha\text{-}C} > \triangle G_{Si} > \triangle G_{SiC}$, the SiC phase is the most stable phase. As the annealing temperature increases, the size of Si-QDs decreases until it disappears, and finally a SiC film is formed.

A photodetector was prepared in order to investigate the photoelectric response characteristics of the Si-QDs film. Fig. 3(a) illustrates the fabrication process of the device. A carbon-silicon composite film was deposited onto a masked n-Si (100) substrate via co-sputtering of C and n-Si targets. After 600 °C annealing, Al electrode was vapor-deposited on the Si-QDs film and n-Si substrate. A window of 2 mm × 2 mm was developed on the electrode to expose the photosensitive surface to improve charge collection. Finally, gold wires were attached to the Al electrodes using silver paste. Schematic diagram and optical image of the device is shown in the inset of Fig. 3(f) and 3(g), respectively. The effect of optical wavelength on the device performance (under 5 V bias) was studied by irradiating the photodetector with 740, 850 and 940 nm light. The measured log *J* against *V* curve is shown in Fig. 3(b). An increase in the device current was evident under light irradiation as compared to dark condition, hence demonstrating good photoelectric response and ohmic contact. However, a better performance was noticeable when the device was irradiated with 940 nm light. Fig. 3(c) shows the log *J* against *V* curve of the photodetector irradiated using 940 nm infrared light with optical power density of 1.1 and 4.3 $mWcm^{-2}$. From the graph, an increase in the photon energy and bias voltage resulted in the increase of the device photocurrent density. The photoelectric conversion efficiency of the detector to the optical signal is represented by spectral responsivity (*R*), which can be calculated using the following equation:

$$R = J_{ph}/P_{opt} \quad (2)$$

where J_{ph} is photocurrent density and P_{opt} is incident optical power density. Fig. 3(f) shows a plot of calculated *R* against *V*. From the plot, it can be seen that *R* reached a maximum value of 7.43 AW^{-1} when P_{opt} was 1.1 $mWcm^{-2}$ at 940 nm light under bias voltage of 5 V. The detection rate (*D**) describes the ability of the device to detect signals, and *R* is

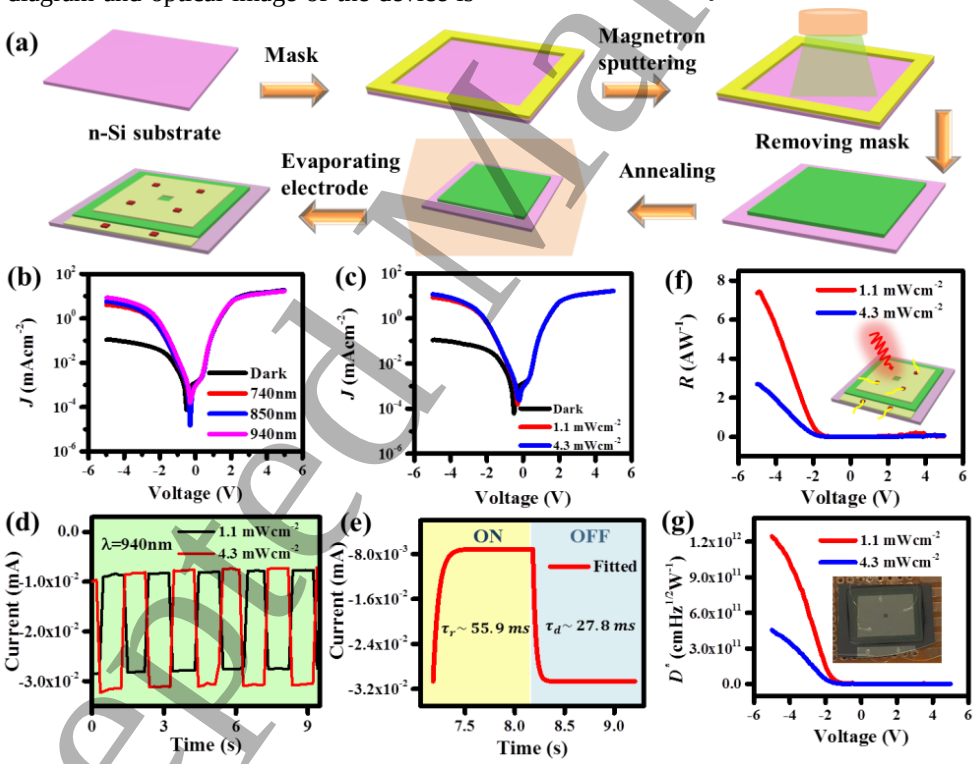

Figure 3. (a) Schematic diagrams illustrating the fabrication process of the photodetector based on Si-QDs film. (b) Plot of log *J-V* curve of the photodetector in the dark and irradiated under different wavelength of light. (c) Plot of log *J-V* curve of the photodetector in the dark and irradiated under 940 nm light at different optical power densities. (f) and (g) Plots of Responsivity (*R*) and Detectivity (*D**) against *V*, respectively. (Inset: schematic diagram and optical image of the device, respectively). (d) Transient response of the photodetector under 940 nm light illumination. (e) Rise and fall times of photogenerated carriers.

the main performance parameter of the detector. D^* can be calculated using the following equation:

$$D^* = \frac{R}{\sqrt{2q|J_{dark}|}} \quad (3)$$

where q is absolute value of electron charge and J_{dark} is dark current density. A plot of calculated D^* against V is shown in Fig. 3(g), which indicates D^* reached a maximum value of 1.246×10^{12} cmHz$^{1/2}$W^{-1} (1 cmHz$^{1/2}$W^{-1} = 1 Jones) when the photodetector was biased at 5 V and irradiated with 940 nm light having a P_{opt} of 1.1 mWcm^{-2}.Therefore, the device exhibited excellent response and detection rates. Furthermore, the device demonstrated good responsiveness and stability under dirrerent light power densities as shown in Fig. 3(d), which displays the transient response of the device under 940 nm light. Fig. 3(e) shows the rise and fall times of 55.9 and 27.8 ms of the photogenerated carriers, respectively.Table 1 compares the performances, such as response spectral range, carrier rise and fall times, responsivity and detectivity, of the device in this work with previously reported photodetectors based on Si-QDs. The values of R and D^* reported in this work were larger than previously reported Si-QDs based photodetectors. In this study, Si-QDs was prepared in situ, and the annealing temperature is relatively low, so that the Si-QDs film has fewer defects, and the photo-generated carrier separation efficiency is high, so the device performance is better. At the same time, the passivation of Si-QDs also leads to reducing the dark current of the device, which results in improving the performance of the device.

Table 1. Comparison of the performances of Si-QDs based photodetectors

Materials	Wavelength (nm)	t_r (ms)	t_f (ms)	R(A/W)	D^*(Jones)	Ref.
Si-QDs/n-Si	940	55.9	27.8	7.43	1.25×10^{12}	This Work
Graphene/Si-QDs /n-Si	500-900	2×10^{-3}	2×10^{-3}	0.32-0.65	4.5×10^{12}	[22]
MLG/Si-QDs	400-1000	$\sim 7 \times 10^{-4}$	$\sim 7 \times 10^{-4}$	0.351	9.42×10^{11}	[23]
Graphene/Si-QDs	400-1000	-	-	0.413	1.09×10^{10}	[24]
Si-QDs/Graphene	400-1000	$\sim 2.5 \times 10^{-5}$	$\sim 2.5 \times 10^{-5}$	0.495	7.4×10^{9}	[25]

4. Conclusion

In conclusion, carbon-silicon composite film was prepared by magnetron sputtering. After annealing at 600 °C for 1 h, the film transformed from an amorphous state to crystalline state, and Si-QDs were precipitated at the surface of the film. However, the Si-QDs disappeared when the film was annealed at higher temperature of 900 °C. This work demonstrated the preparation of Si-QDs film using lower annealing temperature than previously reported. In order to study the photoelectric properties of the Si-QDs film, a photodetector based on Si-QDs film/n-Si was fabricated and characterized. Under a bias voltage of 5 V and irradiation of 940 nm light, R and D^* of the device reached a maximum value of 7.43 AW^{-1} and 1.246×10^{12} cmHz$^{1/2}$W^{-1}, respectively. The transient response of the device irradiated at 940 nm also exhibited good stability. Hence, the Si-QDs film demonstrated great potential in the development of high-performance infrared photodetectors.

See Supplementary Materials for EDS spectrum of the as-grown film (Supplementary Figure S1),TEM image of the 600 °C annealed film (Supplementary Figure S2), XPS spectrum of the film after annealing at 600 °C (Supplementary Figure S3), TEM images of the film before and after annealing (Supplementary Figure S4) and performance of the device after one month without device package (Supplementary Figure S5).

Acknowledgements

This work was supported by National Natural Science Foundation of China (Grant Nos. 61106098 and 51462037) and Yunnan Key Laboratory of Advanced Photoelectric Materials & Devices, China.

References

[1] Sagnes I, Halimaoui A, Vincent G and Badoz P A 1993 Optical absorption evidence of a quantum size effect in porous silicon *Appl. Phys. Lett.* **62** 1155

[2] Ball P, Garwin L 1992 Science at the atomic scale *Nature* **355** 761

[3] Leon R, Petroff P M, Leonard D and Fafard S 1995 Spatially resolved visible luminescence of self-assembled semiconductor quantum dots *Science* **267** 5206

[4] Caldeira A O, Leggett A 1981 Influence of dissipation on quantum tunneling in macroscopic systems *Phys. Rev. Lett*. **46** 211

[5] Spanhel L, Haase M, Weller H, Henglein A 1987 Cheminform abstract: photochemistry of colloidal semiconductors. part 20. surface modification and stability of strong luminescing CdS particles *J. Am. Chem. Soc*. **109** 5649

[6] Darbandi M, Thomann R, Nann T 2005 Single quantum dots in silica spheres by microemulsion synthesis *Chem. Mater*. **17** 5720

[7] Gaponik N, Talapin D V, Rogach A L, Eychmüller A and Weller H 2002 Efficient phase transfer of luminescent thiol-capped nanocrystals: from water to nonpolar organic solvents *Nano Lett*. **2** 803

[8] Kang Z, Yang L, Tsang C H A, Ma D D D and Lee S T 2010 Cheminform abstract: water-soluble silicon quantum dots with wavelength-tunable photoluminescence *ChemInform* **40** 661

[9] Barik S, Tan H H, Jagadish C 2006 Comparison of InAs quantum dots grown on GaInAsP and InP *Nanotechnology* **17** 1867

[10]Gourbilleau F, Portier X, Ternon C, Voivenel P and Rizk R 2001 Si-rich/SiO_2 nanostructured multilayers by reactive magnetron sputtering *Appl. Phys. Lett*. **78** 3058

[11]Budiman M F, Hu W, Igarashi M, Tsukamoto R., Isoda T and Itoh, K M et al. 2012 Control of optical bandgap energy and optical absorption coefficient by geometric parameters in sub-10 nm silicon-nanodisc array structure *Nanotechnology* **23** 065302

[12]Cao Y Q, Xin X U, Shuxin L I, Wei L I, Jun X U and Chen K 2013 Improved photovoltaic properties of Si quantum dots/SiC multilayers-based heterojunction solar cells by reducing tunneling barrier thickness *Frontiers of Optoelectronics* **6** 228

[13]Rezgui B, Sibai A, Nychyporuk T, Lemiti M, Bremond G, Maestre D and Palais O 2010 Effect of total pressure on the formation and size evolution of silicon quantum dots in silicon nitride films *Appl. Phys. Lett*. **96** 125419

[14]So Y H, Gentle A, Huang S, Conibeer G, Green M A 2011 Size dependent optical properties of Si quantum dots in Si-rich nitride/Si_3N_4 superlattice synthesized by magnetron sputtering *Journal of Applied Physics* **109** 1046

[15]Chen X, Yang P 2014 Density improvement of Si quantum dots embedded in Si-rich silicon nitride films by light-filtering rapid thermal processing *Journal of Materials Science Materials in Electronics* **25** 5410

[16]Joo B S, Jang S, Gu M, Jung N, Han M 2019 Effect of auger recombination induced by donor and acceptor states on luminescence properties of silicon quantum dots/SiO_2 multilayers *Journal of Alloys and Compounds* **801** 568

[17]Seifarth H, Schmidt J U, Grötzschel R, Klimenkov M 2001 Phenomenological model of reactive r.f.-magnetron sputtering of Si in Ar/O_2 atmosphere for the prediction of SiO_x thin film stoichiometry from process parameters *Thin Solid Films* **389** 108

[18]Jiang C W, Green M A 2006 Silicon quantum dot superlattices: modeling of energy bands, densities of states, and mobilities for silicon tandem solar cell applications *J. Appl. Phys*. **99** 4006

[19]Wen G, Zeng X, Wen X, Liao W 2014 Photoluminescence properties and crystallization of silicon quantum dots in hydrogenated amorphous si-rich silicon carbide films *Journal of Applied Physics* **115** 155704

[20]Swain B P 2006 The analysis of carbon bonding environment in HWCVD deposited a-SiC:H films by XPS and Raman spectroscopy *Surface & Coatings Technology* **201** 1589

[21]Yang D Q, Gillet J N, Meunier M, Sacher E 2005 Room temperature oxidation kinetics of Si nanoparticles in air, determined by x-ray photoelectron spectroscopy *J. Appl. Phys*. **97** 440

[22]Shin D H, Jang C W, Kim J M and Choi S H 2018 Self-powered Ag-nanowires-doped graphene/Si quantum dots/Si heterojunction photodetectors *Journal of Alloys & Compounds* **758** 32

[23]Dong H S, Dong H J and Choi S H 2019 High-detectivity and-stability multilayer-graphene/Si-quantum-dot photodetectors with TiO_x back-surface passivation layer *Dyes and Pigments* **170** 107587

[24]Shin D H, Jang C W, Kim J H, KimJ M, Lee H S, Seo S W et al 2017 Enhancement of efficiency and long-term stability in graphene/Si-quantum-dot heterojunction photodetectors by employing bis(trifluoromethanesulfonyl)-amide as a dopant for graphene *J. Mater. Chem. C.* **10** 1039

[25]Yu T, Wang F, Xu Y, Ma L, Pi X and Yang D 2016 Graphene coupled with silicon quantum dots for high-performance bulk-silicon-based schottky-junction photodetectors *Adv Mater* **28** 4912